

Development and validation of a novel artificial intelligence driven tool for accurate mandibular canal segmentation on CBCT

Pierre Lahoud^{a,b,*}, Siebe Diels^c, Liselot Niclaes^a, Stijn Van Aelst^a, Holger Willems^c,
Adriaan Van Gerven^c, Marc Quirynen^b, Reinhilde Jacobs^{a,d}

^a OMFS-IMPACT Research Group, Department of Imaging and Pathology, Faculty of Medicine, KU Leuven & Department of Oral and Maxillofacial Surgery, University Hospitals Leuven, Belgium

^b Department of Oral Health Sciences, Periodontology and Oral Microbiology, University Hospitals of Leuven, Belgium

^c Relu BV, Leuven, Belgium

^d Department of Dental Medicine, Karolinska Institute, Stockholm, Sweden

ARTICLE INFO

Keywords:

Artificial intelligence
Inferior alveolar nerve
Neural network models
Cone-beam computerized tomography

ABSTRACT

Objectives: The objective of this study is the development and validation of a novel artificial intelligence driven tool for fast and accurate mandibular canal segmentation on cone beam computed tomography (CBCT).

Methods: A total of 235 CBCT scans from dentate subjects needing oral surgery were used in this study, allowing for development, training and validation of a deep learning algorithm for automated mandibular canal (MC) segmentation on CBCT. Shape, diameter and direction of the MC were adjusted on all CBCT slices using a voxel-wise approach. Validation was then performed on a random set of 30 CBCTs - previously unseen by the algorithm - where voxel-level annotations allowed for assessment of all MC segmentations.

Results: Primary results show successful implementation of the AI algorithm for segmentation of the MC with a mean IoU of 0.636 (± 0.081), a median IoU of 0.639 (± 0.081), a mean Dice Similarity Coefficient of 0.774 (± 0.062). Precision, recall and accuracy had mean values of 0.782 (± 0.121), 0.792 (± 0.108) and 0.99 ($\pm 7.64 \times 10^{-05}$) respectively. The total time for automated AI segmentation was 21.26 s (± 2.79), which is 107 times faster than accurate manual segmentation.

Conclusions: This study demonstrates a novel, fast and accurate AI-driven module for MC segmentation on CBCT. **Clinical Significance:** Given the importance of adequate pre-operative mandibular canal assessment, Artificial Intelligence could help relieve practitioners from the delicate and time-consuming task of manually tracing and segmenting this structure, helping prevent pre- and post-operative neurovascular complications.

1. Introduction

The last two decades have seen a shift towards full digital workflows for pretreatment diagnostics, treatment planning and follow-up [1,2]. In this regard, Cone Beam Computed Tomography (CBCT) has gained a prominent position in this workflow, considering the low costs and compact size of such machines, meanwhile providing essential 3D anatomical details with high spatial resolution and low radiation dose [2,3]. CBCT allows visualization of critical anatomical structures, such as the mandibular canal (MC), housing the vital mandibular neurovascular bundle [4,5]. Knowledge of the exact position of the MC and its relation to adjacent structures is crucial to help avoiding mild to severe life-altering conditions [4–6] during implant placement [4,5], sagittal

split osteotomy [4,7], cyst removal [4,8] and tooth extraction [4,5,7,9]. Such injuries are relatively common (incidence from 0.2 to 8.4%) [9, 10], and could lead to (semi)-permanent paresthesia, anesthesia or dysesthesia of the innervated structures of the affected side (such as lip, jaw, teeth, tongue, mucosa, gingiva) [4,8]. Iatrogenic trigeminal damage could also significantly impact quality of life, lifestyle and psychosocial outcomes [11].

Accurate pre-operative assessment of the MC and any potential anatomical variation of this structure is thus crucial to avoid post-operative complications and damage to the inferior alveolar nerve [4, 7]. Yet, precise and automatic delineation of the MC remains challenging. Several CBCT-guided planning software tools allow for visualization of the MC after manual placement of marks at different locations

* Corresponding author.

E-mail address: pierre.lahoud@kuleuven.be (P. Lahoud).

<https://doi.org/10.1016/j.jdent.2021.103891>

Received 26 September 2021; Received in revised form 29 October 2021; Accepted 11 November 2021

Available online 13 November 2021

0300-5712/© 2021 Elsevier Ltd. All rights reserved.

across the canal's path with interpolation into a fixed diameter cylinder, providing a virtual depiction the MC, denoted as MC tracing.

Nevertheless, this approach yields certain inherent inaccuracies given the fully manual nature of the tracing [12,13], coupled with the inherent limitations of CBCTs in terms of low image contrast, increased noise, artefacts and the lack of Hounsfield units. All of this adds to the complexity of achieving - manually or automatically - an accurate assessment of this structure [3,14].

For these reasons, the introduction of Convolutional Neural Networks (CNNs) and Artificial Intelligence (AI) in medical imaging segmentation tasks has been seen as an apparent solution for countering such problems: CNNs, which are at the core of AI technologies, are computational processing systems heavily inspired by how the occipital cortex operates. They are comprised of neurons that self-optimize through learning, consisting of an input and an output layer, with multiple hidden layers in between. They are primarily used in the field of patterns recognition within images [15].

CNNs and AI have proven to counter various limitations previously met with manual and automatic segmentation methods [16–18], which could in our case allow for accurate automated segmentation of the MC, in spite of localized morphological variations such as bifid canals and localized canal enlargement, assisting clinicians in accurate presurgical MC assessment; thus lowering the risk of per-and postoperative complications.

Therefore, the aim of this study is twofold: 1. development and validation of a novel tool for accurate voxel-wise segmentations, capable of adjusting to variations in MC shape and width MC; 2. training and automation of such a tool for fast and accurate result generation. The hypothesis is that such AI-driven tool might provide MC segmentations for clinical use, that are much faster and at least as accurate as the expert's segmentations.

2. Materials and Methods

2.1. Data acquisition and training database

A random collection of CBCT scans from the M3BE database (Ethical Committee Research UZ/KU Leuven B322201525552) was initially gathered, yielding a total of 235 CBCT scans from dentate patients needing oral surgical procedures (mean age 25±11 years old). Scans were acquired using the 3D Accuitomo 170 (Morita, Kyoto, Japan), ProMax 3D MAX (Planmeca, Helsinki, Finland), Scanora 3Dx (Soredex, Tuusula, Finland) and NewTom VGI EVO (QR Verona, Cefla, Verona, Italy) devices (Table 1). An initial anonymization of the image dataset was subsequently performed.

The initially collected dataset was divided as follow: 166 cases for training (70.64%), 39 cases for testing (16.59%) and 30 cases for final validation of the algorithm (12.77%). All three subsets included a random distribution of CBCT scans from the four scanning devices, having various acquisition parameters and degrees of artefacts.

The testing dataset allowed to test several CNNs and opt for the one that showed the best results for the various parameters, such as speed and accuracy [19].

Next, the chosen CNNs were trained using a large number of cases (training dataset). To tackle maximum variability and increase robustness of the algorithm, included CBCTs relied on a variety of field of view (FOV) dimensions, various voxel sizes, presence of different types of artefacts in the scans, low- and high-resolution images, many levels of scattering and different degrees of mandibular canal cortication. The trained model was finally tested for validation using a set of unseen cases by the algorithm - being the validation dataset.

As for the training of the algorithm, 40 random CBCT scans were initially imported into Romexis® version 5.2.1.R (Planmeca, Helsinki, Finland) for tracing of the MC - going from the mandibular foramen until the mental foramen - using the built-in tool in Romexis® for nerve annotation (Fig. 1.A). The MC tracings were performed and verified by

Table 1

Acquisition devices and parameters of the study's database.

| CBCT Device | Voxel Size µm | Field of View (FOV) mm | mm x | Number of Cases |
|-------------------|------------------|---------------------------|------|--------------------|
| NewTom VGI evo | 100 | 80 x 80 | | 4 |
| NewTom VGI evo | 125 | 120 x 80 | | 7 |
| NewTom VGI evo | 150 | 80 x 80 | | 5 |
| NewTom VGI evo | 150 | 120 x 80 | | 4 |
| NewTom VGI evo | 200 | 120 x 80 | | 61 |
| NewTom VGI evo | 200 | 100 x 100 | | 26 |
| NewTom VGI evo | 250 | 150 x 120 | | 24 |
| NewTom VGI evo | 300 | 240 x 190 | | 51 |
| NewTom VGI evo | 300 | 160 x 160 | | 3 |
| ProMax 3D MAX | 250 | 130 x 90 | | 5 |
| ProMax 3D MAX | 400 | 230 x 260 | | 7 |
| ProMax 3D MAX | 200 | 130 x 130 | | 5 |
| Accuitomo 170 | 250 | 140 x 165 | | 16 |
| Accuitomo 170 | 200 | 140 x 100 | | 7 |
| Accuitomo 170 | 125 | 100 x 100 | | 5 |
| Scanora 3Dx | 160 | 140 x 100 | | 2 |
| Scanora 3Dx | 250 | 170 x 120 | | 3 |
| | | | | 235 |

two experts in dentomaxillofacial radiology. The tool required the user to specify control points for the canal, followed by an automated interpolation of the pathway of the MC, based on the control points [20]. A uniform cylinder of 2.50 mm was then fixed to simulate the width of the mandibular canal [21] (Fig. 1.B). This initial training set allowed for the development of an initial version of a Deep Learning (DL) algorithm, Virtual Patient Creator (Relu BV, Leuven, Belgium), capable of performing accurate voxel-wise MC segmentations. 126 new random CBCT scans were then imported into the DL tool (Fig 1.C), where two experts in dentomaxillofacial radiology accurately segmented the limits of the MC on cross-sectional slices, with a voxel-wise segmentation approach (Fig. 1.D).

The performed segmentations were double checked jointly by the experts and adjustments were made when deemed necessary. Segmentations were then used to train and refine the DL algorithm and allow for the development of a refined and robust algorithm (Fig. 1.E).

2.2. Dataset pre-processing and augmentation

Various types of data augmentation strategies were applied to artificially increase the dataset and improve on generalizability and robustness of the model (Fig. 1.B, D). These strategies included affine transformations such as scaling, rotation, shear, mirroring, translation, elastic deformations and random cropping. These techniques were randomly applied during the training phase.

2.3. Network architecture of the convnet

In this study, two CNNs worked together in order to produce a full-resolution segmentation output. The first CNN performed a coarse segmentation of the MC, while the second CNN performed in turn a fine segmentation on the region around the coarse segmentation.

Based on the test set - which is used to optimize the network architecture by minimizing the error on this dataset [22] - the architecture used for MC segmentation was a 3D U-Net [17,23]. The U-Net is an encoder-decoder fully convolutional network with skip connections, that has been successfully applied in various medical segmentation

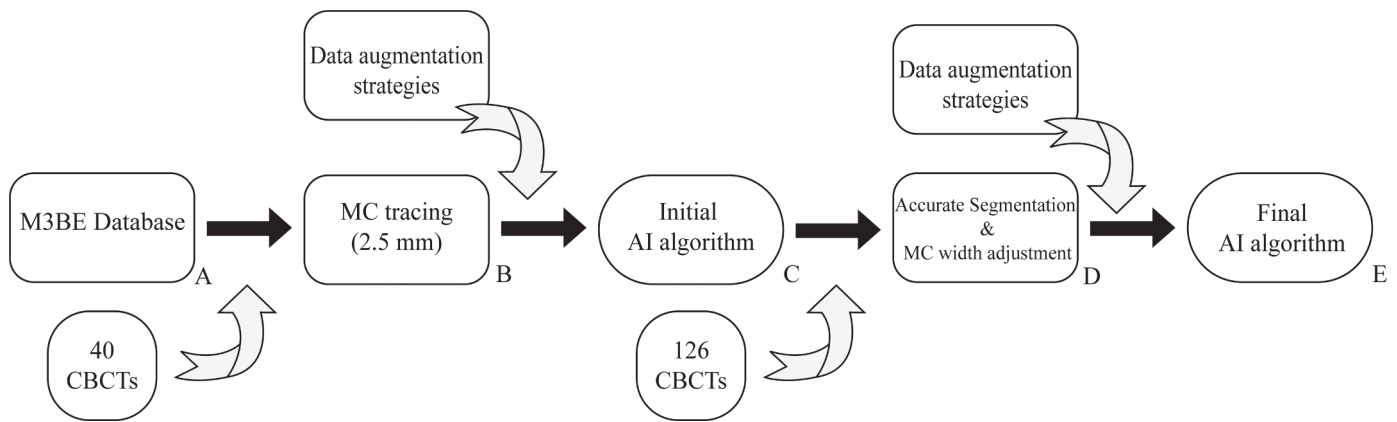


Fig. 1. Workflow of the methodology used for the development and training of an AI-driven algorithm for mandibular canal segmentation on CBCT.

problems. The encoder extracted the interesting features from the input image using convolutions, rectified linear unit (ReLU) operation and max pooling. The images were then down-sampled, resulting in a final feature map containing global information about the image. The decoder used is symmetric to the encoder and helps generate a dense segmentation mask of the input.

To improve localization of the network, skip connections were added to combine the feature maps from the decoder with the ones of the encoder. A semantic segmentation branch subsequently combined the feature maps from all the layers of the decoder into one single output. Feature maps were up-sampled to the same size using convolutions, group norm, ReLU and bilinear up-sampling – and then combined using element-wise summing. The model was trained on full resolution patches with Binary Cross Entropy loss and early stopping (Fig. 2).

2.4. AI driven MC segmentation

A 3D U-Net CNN [23], trained with the above described dataset was

developed for automated detection and segmentation of the MC. The tool relied on automatically detecting the path of the MC using a voxel-wise probability approach.

Moreover, the possibility of user interaction was preserved with the ability to modify the path of the canal as well as its shape and width. Over- and under-estimations could therefore be adjusted, if deemed necessary by the operator.

2.5. Validation dataset

AI study validation relied on 30 randomly selected CBCT scans, where AI-driven segmentation of the MC was performed (Fig. 3).

Results were saved as Digital Imaging and Communications in Medicine (DICOM) files and as Standard Tessellation Language file (STL). Expert manual segmentations were then conducted, allowing for further objective accuracy assessment between AI-driven versus expert manual MC segmentations.

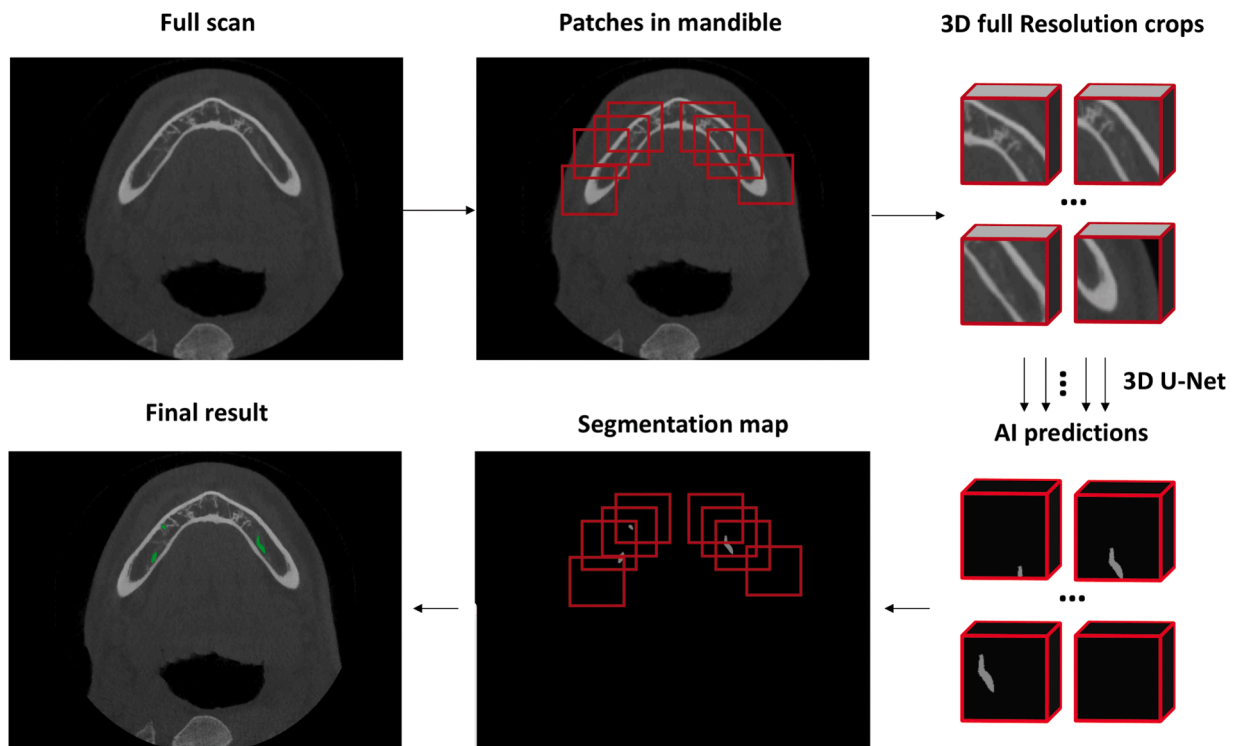


Fig. 2. Workflow of the 3D U-Net Convolutional Neural Network.

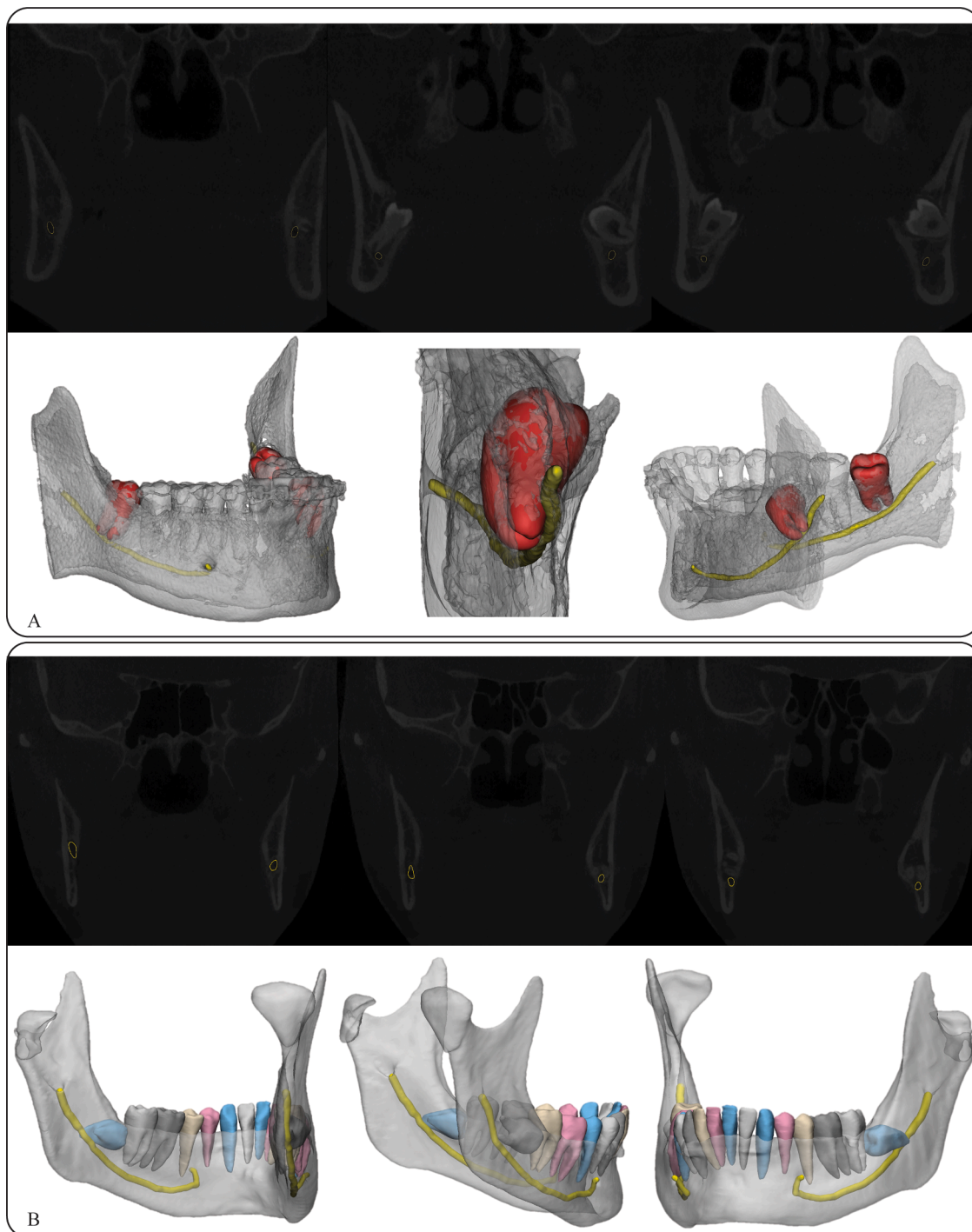


Fig. 3. 3-Dimensional simulation of an AI-driven mandibular canal segmentation on CBCT, where the proximity between the mandibular canal and third molar can be visualized and assessed preoperatively (A), as well as its relation with all dental structures in the mandible (B).

2.6. Assessment and validation of the algorithm

Voxel-level annotations were performed on the validation set to assess the accuracy and performance of the AI-driven segmentations. Firstly, the intersection-over-union (IoU) score was assessed: IoU is a standard performance measure for the object category segmentation problem. For a given object, the IoU measures the similarity between the predicted object and its ground-truth counterpart. It is defined by the following equation:

$$IoU = \frac{TP}{FP + TP + FN} \tag{1}$$

where, TP, FP, and FN denote the true positive, false positive and false negative pixel counts, respectively [24]. The area of overlap between expert-user and AI-algorithm results is where the algorithm identifies which voxels exactly match the annotated ground truth segmentation. These voxels are known as TP. The voxels erroneously segmented by the CNN are known as FP and the pixels that the CNN failed to segment are known as FN.

Furthermore, the Dice Similarity Coefficient (DSC), which relates to

the amount of intersection between two segmented objects [16,24], is defined by the following equation:

$$DSC = \frac{2 \times TP}{(TP + FP) + (TP + FN)} \quad (2)$$

Hausdorff Distance (HD) was used as an indicator of the largest segmentation error [25]. HD indicates the longest distance given from a point in the first segmented entity (manual expert segmentation) to its closest point in the other entity (AI-computed segmentation). HD is therefore computed between boundaries of the AI-computed and ground-truth segmentations, which consist of curves in 2D and surfaces in 3D [25,26]. HD is defined by:

$$HD(A, B) = \max[hd(A, B), hd(B, A)]$$

Where the function $hd(A, B)$ is referred to as the directed Hausdorff distance from A to B. It ranks each point of A according to its distance to the nearest point of B. The largest of these distances determines the value of $hd(A, B)$ [26].

The precision and recall measures characterize the agreement between the oriented boundary edge elements of region boundaries of two segmentations [27]. They are therefore calculated based on overlapping regions. Two aspects related to overlapping regions are stated prior to experimentation: the matching direction and the corresponding criteria. The matching direction for the precision measure is defined as a reference-to-segment directional correspondence [28]. Precision and recall measures relate to the following equations:

$$Precision = \frac{TP}{TP + FP}$$

$$Recall = \frac{TP}{TP + FN}$$

Accuracy is a weighted arithmetic mean which explicitly takes into account the classification of negatives, and is expressible both as a weighted average of Precision and Inverse Precision and as a weighted average of Recall and Inverse Recall [29]. It is defined as follows:

$$Accuracy = \frac{TP + TN}{TP + TN + FP + FN}$$

Time was also recorded by from the moment the algorithm received the DICOM of the scan, until a segmentation map was outputted.

2.7. Part comparison analysis of MC segmentation versus tracing

In order to further elaborate on the advantages of the development of a MC segmentation tool as opposed to MC tracing – where a fixed diameter is used to simulate the whole path of the neurovascularization, a part comparison analysis was performed based on the two methods: For the AI-driven automatic MC segmentation method, the DICOM files were imported into the cloud-based tool, where the AI-driven algorithm yielded stereolithography (STL) files of the segmented MC. The same DICOM files were then loaded into Romexis® version 5.2.1.R, where accurate manual MC tracing was performed, relying on a 2.5 mm fixed diameter and a 2.0 mm slice thickness between the different points of the tracing. After export, STLs were imported into 3-Matic (materialise, Leuven, Belgium), where a signed part comparison analysis (PCA) was performed.

PCA allows to calculate the volumetric deviation between two structures: in this case between AI-driven segmentations and manual MC

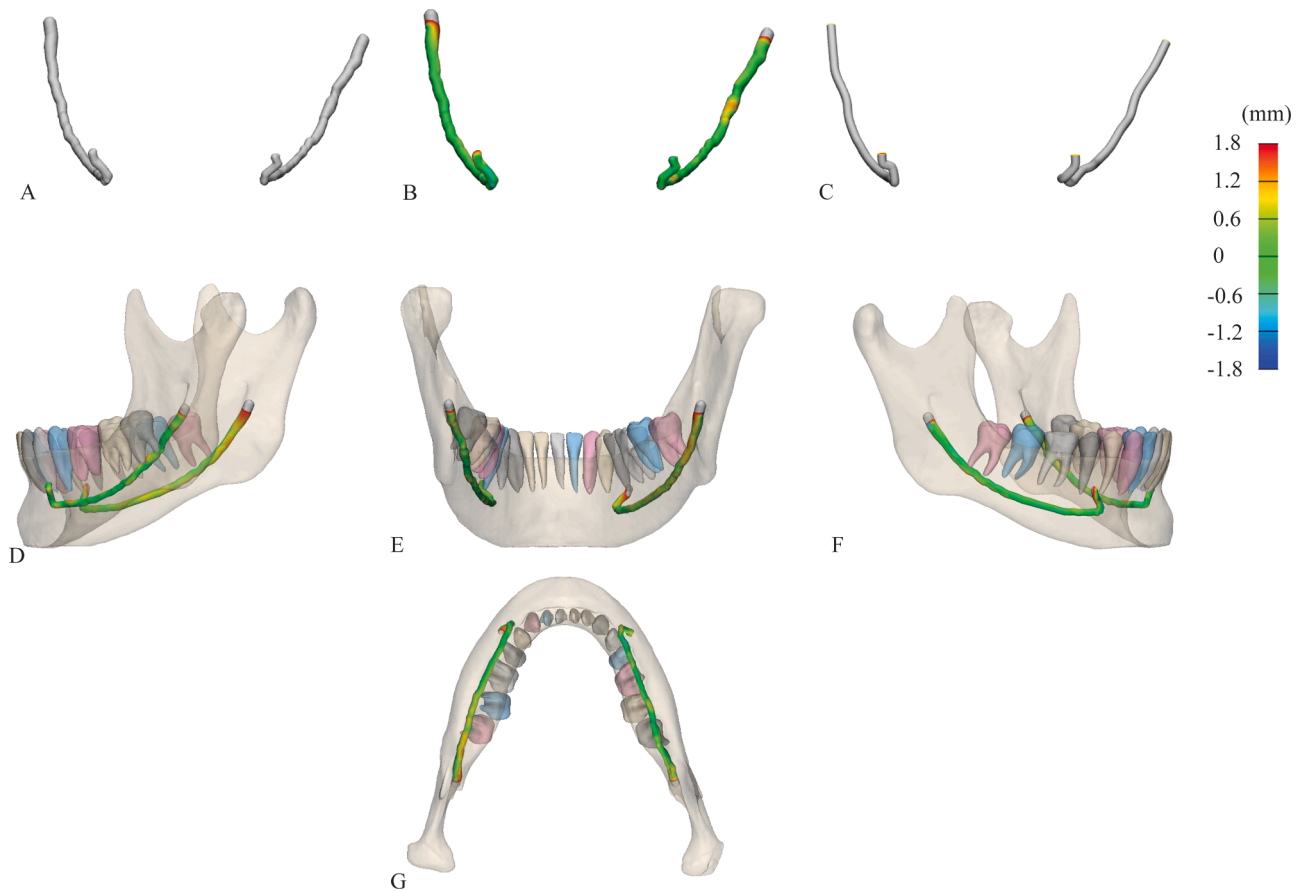


Fig. 4. 3-Dimensional part comparison analysis (B) between mandibular canal segmentations (A) and mandibular canal tracing (C). Lateral (D, F), frontal (E) and inferio-superior (G) views of the part comparison analysis highlight areas of deviation between the two scenarios, due to local variation of the width of the mandibular canal, inferior or superior to 2.5 mm.

tracing (Fig. 4).

3. Results

Results of IoU, DSC, Precision, Recall, Accuracy and HD can be found in Table 2. The mean IoU of the 30 cases was 0.636 (± 0.081), the median IoU 0.639 (± 0.081), the mean DSC was 0.782 (± 0.062). HD had a mean value of 0.705 mm (± 0.389), while Precision, Recall and Accuracy had mean values of 0.782 (± 0.121), 0.792 (± 0.108) and 0.99 ($\pm 9.52 \times 10^{-05}$) respectively Total time from uploading until result visualization was 21.26 s (± 2.79), while the average time for expert manual segmentation was 37.9 min (± 9.11).

Furthermore, a part comparison analysis from the registration of the AI-driven MC segmentation on the expert manual segmentations shows high agreement between the two methods at the level of first and second molars, as well as at the distal level of the second molar, mesial to the first molar and at the level of the mandibular foramen, with a mean deviation of 0.382 mm (± 0.860) between AI-driven automated segmentations and manual tracing of the MC (Fig. 4).

4. Discussion

Accurate MC assessment for procedures similar to tooth extraction, implant placement, bone grafting and orthognathic surgeries have proven to be of high clinical relevance [13,20,30]. Assessing structures using imaging modalities, such as CBCTs can be done through segmentation.

However, limitations of conventional segmentation techniques for surgical assessment in both the medical and dental fields have led in the last few years to a surge in DL technologies for classification and segmentation purposes [31,32]. CNNs have shown great potential in

Table 2

Results of the intersection-over-union (IoU), Dice Similarity Coefficient (DSC), Precision, Recall, Accuracy and Hausdorff distance (HD) (mm) measures are presented for all 30 CBCT scans of the validation dataset. The mean and standard deviation (SD) of the results are shown in the last two rows.

| | IoU | DSC | Precision | Recall | Accuracy | HD |
|-------------|--------------|--------------|--------------|--------------|---|--------------|
| 1 | 0.716 | 0.835 | 0.834 | 0.835 | 0.999 | 0.559 |
| 2 | 0.785 | 0.880 | 0.915 | 0.846 | 0.999 | 0.346 |
| 3 | 0.652 | 0.789 | 0.916 | 0.694 | 0.999 | 0.600 |
| 4 | 0.688 | 0.815 | 0.750 | 0.892 | 0.999 | 0.400 |
| 5 | 0.672 | 0.804 | 0.719 | 0.912 | 0.999 | 0.447 |
| 6 | 0.698 | 0.822 | 0.888 | 0.765 | 0.999 | 0.400 |
| 7 | 0.504 | 0.670 | 0.577 | 0.799 | 0.999 | 1.095 |
| 8 | 0.695 | 0.820 | 0.709 | 0.972 | 0.999 | 0.400 |
| 9 | 0.637 | 0.778 | 0.923 | 0.673 | 0.999 | 0.559 |
| 10 | 0.449 | 0.620 | 0.708 | 0.551 | 0.999 | 2.163 |
| 11 | 0.634 | 0.776 | 0.788 | 0.765 | 0.999 | 0.600 |
| 12 | 0.519 | 0.683 | 0.549 | 0.906 | 0.999 | 1.637 |
| 13 | 0.547 | 0.707 | 0.852 | 0.605 | 0.999 | 0.938 |
| 14 | 0.630 | 0.773 | 0.732 | 0.818 | 0.999 | 0.632 |
| 15 | 0.640 | 0.781 | 0.889 | 0.696 | 0.999 | 0.600 |
| 16 | 0.780 | 0.876 | 0.915 | 0.841 | 0.999 | 0.490 |
| 17 | 0.595 | 0.746 | 0.600 | 0.987 | 0.999 | 0.490 |
| 18 | 0.513 | 0.678 | 0.545 | 0.896 | 0.999 | 0.825 |
| 19 | 0.546 | 0.706 | 0.579 | 0.906 | 0.999 | 1.020 |
| 20 | 0.589 | 0.741 | 0.757 | 0.727 | 0.999 | 0.938 |
| 21 | 0.664 | 0.798 | 0.814 | 0.783 | 0.999 | 0.500 |
| 22 | 0.698 | 0.822 | 0.828 | 0.816 | 0.999 | 0.490 |
| 23 | 0.626 | 0.770 | 0.841 | 0.710 | 0.999 | 0.849 |
| 24 | 0.673 | 0.805 | 0.757 | 0.858 | 0.999 | 0.490 |
| 25 | 0.614 | 0.761 | 0.846 | 0.691 | 0.999 | 0.600 |
| 26 | 0.643 | 0.783 | 0.731 | 0.843 | 0.999 | 0.896 |
| 27 | 0.752 | 0.859 | 0.858 | 0.859 | 0.999 | 0.447 |
| 28 | 0.724 | 0.840 | 0.924 | 0.770 | 0.999 | 0.400 |
| 29 | 0.598 | 0.748 | 0.969 | 0.609 | 0.999 | 0.748 |
| 30 | 0.591 | 0.743 | 0.758 | 0.729 | 0.999 | 0.600 |
| Mean | 0.636 | 0.774 | 0.782 | 0.792 | 0.999 | 0.705 |
| SD | 0.081 | 0.062 | 0.121 | 0.108 | 9.52×10^{-5} | 0.389 |

generating accurate results, given their capabilities of learning from contextual information within image slices of complex 3D anatomical structures [33]. Nowadays, CNNs have proven to outperform conventional approaches in many computer-vision and image segmentation tasks [23,31,32]. While current limitations were mainly centered around GPU and hardware technicalities, current progresses - as is the case in this study - allow to run DL algorithms on the cloud, relieving clinicians and researchers from having to invest and maintain complex and expensive hardware equipment.

This study reports on development and validation of a novel tool for MC segmentation based on DL and AI technologies. In this study, the algorithm successfully detected the presence of the MC bilaterally on all CBCTs. Despite the heterogeneity of the dataset used in terms of CBCT devices, FOVs, voxel sizes, presence of artefacts and the various degrees of cortication of the MC, a high level of accuracy was achieved by the algorithm, with only one case from the validation subset displaying an IoU < 0.5 (supplemental Fig. 1).

Regarding accuracy metrics, it must be stated that the IoU penalizes slight shifts in overlap quite heavily, with a good overlap having an IoU > 0.60 (DSC > 0.75) [34].

Kwak et al. in [30] tested several CNNs for mandibular canal detection and obtained a mean IoU of 0.577 using a 3D U-Net. Their study however shows a lack of variability in the acquisition parameters of the training set, whereas all CBCT scans were acquired using the same device, with relatively similar acquisition parameters. This issue was tackled in the present study, where variability was greatly introduced in the training, testing and validation datasets, as well as by the used of data augmentation strategies, which resulted in a highly robust algorithm with an increased generalizability and performance of the model. As for the study published by Jaskari et al. in [20], results showed a mean DSC of 0.570, well below the acceptable DSC score of 0.75 [34].

With a DSC score of 0.774 (± 0.061), this study relates to the first AI-driven tool for MC segmentation to pass the barrier of clinically acceptable accuracy and allows for its potential use in surgical planning scenarios.

To achieve such results, accurate manual segmentations took expert operators on average 37.9 (± 9.11) minutes per CBCT. Presently, AI-driven automated segmentations of the MC take on average 21.26 s (± 2.79) – 107 times faster than accurate expert-manual segmentation of this bilateral structure.

It is also important to mention that the state-of-the-art approach used in this study relies on accurate MC segmentation as opposed to MC tracing – the latter being the current standard for both manual and automated approaches. MC segmentation allows for more accurate results and the ability to detect and adapt to morphological variations, such as localized canal enlargement and bifid canals.

While a part comparison analysis further confirmed the high agreement in terms of accuracy between MC tracing and MC segmentation (mean deviation of 0.38 mm (± 0.86)), it interestingly illustrated that most deviations happened at the level of the third molar and between first and second premolars. In this context, it is clinically very relevant to highlight that AI-driven segmentations seemed to better adjust in cases where a lack of clear cortication of the MC was observed and in cases of proximity between the roots of the mandibular third molar and the MC when compared to other MC tracing modalities [20]. To further tackle this issue during training, the radiologists cross-checked manual segmentations until reaching a consensus regarding the path of the mandibular canal, before feeding the data to the deep learning algorithm. This allowed to limit potential errors in the training dataset and improve the performance of the algorithm, given that those regions remain of utmost importance for both oral and maxillofacial surgeries, where small anatomical variations might cause mild to severe per- and postoperative complications [4–6] (see also Figs. 3-4).

Blind to the device or acquisition parameters used – the algorithm seemed to perform best on CBCTs, where a higher degree of cortication was observed; from which the algorithm could accurately detect the

presence of the mandibular canal on slices where cortication is visible, and subsequently accurately interpolate the position of the canal in between. Higher degrees of cortication of the MC were observed on CBCTs acquired using a High Resolution (HR) acquisition protocol; a finding that was further supported by Zaki et al. [35].

This study therefore introduces two novel concepts for MC assessment: segmentation using adjustable diameters and shapes for accurate segmentation, as well as automation using AI. This opens new doors in the field of digital dentistry – be it for implant placement, tooth extraction and/or orthognathic surgeries – where future research could help segment anterior branches of the mandibular neuro-vascular bundle up to the mandibular symphysis. Furthermore, AI could assist in automatically classifying and notifying clinicians of any potential proximity and risk associated with a given procedure.

Despite the mandibular canal being one of the most challenging structures to segment on CBCT [30], results obtained in this study point to the benefits AI and DL technologies could bring to both researchers and practitioners in terms of high precision, low time-consumption and user-friendliness for diagnostics, surgical planning and patients' follow-up.

While AI may never fully replace experienced clinicians in their assessments, current results confirm its positive role in assisting both experienced and novice practitioners in their diagnoses, presurgical planning and daily patient management.

This study does however have some limitations: since dealing with Artificial Intelligence requires a great deal of variability, predictions cannot be made as for how the algorithm will perform outside scans taken from the CBCT devices used for training and testing of this study, as well as outside the acquisition parameters used. Anatomical variations are also another aspect where rigorous testing remains needed given the scarcity, yet crucial importance of assessing such variations. Future prospective of this study will focus on tackling these issues as well as on the subsequent segmentation of the anterior portion of the mandibular canal and on scans of adolescent patients presenting mixed dentition.

This will in turn allow for the clinical usability of such a tool in planning oral and maxillofacial surgeries, helping avoid neuro-vascular complications and potentially help in the diagnosis of pathological processes affecting the neurovascular mandibular bundle.

5. Conclusion

The present study introduced development and validation of a novel AI-driven tool for fast and accurate mandibular canal segmentation on CBCT. The results obtained in this study could help improving pre-surgical planning procedures, such as for implant placement, bone grafting, orthognathic surgery and tooth extraction. The developed technique may open further doors for advanced AI development to automatically visualize accessory canals, anatomical variations as well as neurovascularisation in the symphyseal area of the mandible.

6. CRediT authorship contribution statement

P. Lahoud: Conceptualization, Methodology, Validation, Formal Analysis, Investigation, Interpretation, Writing - Original Draft, Writing - Review & Editing.

S. Diels: Conceptualization, Methodology, Validation, Software, Writing - Original Draft, Writing - Review & Editing.

L. Niclaes: Formal Analysis, Investigation, Interpretation, Writing - Review & Editing.

S. Van Aelst: Formal Analysis, Investigation, Interpretation, Writing - Review & Editing.

H. Willems: Conceptualization, Methodology, Software, Writing - Review & Editing.

A. Van Gerven: Conceptualization, Methodology, Software, Validation, Writing - Review & Editing.

M. Quiryren: Conceptualization, Methodology, Interpretation, Writing - Review & Editing.

R. Jacobs: Conceptualization, Methodology, Validation, Interpretation, Writing - Review & Editing.

All authors gave their final approval and agree to be accountable for all aspects of the work.

Declaration of Competing Interest

The authors declare that they have no known competing financial interests or personal relationships that could have appeared to influence the work reported in this paper.

Supplementary materials

Supplementary material associated with this article can be found, in the online version, at doi:10.1016/j.jdent.2021.103891.

References

- [1] R. Jacobs, Dental cone beam CT and its justified use in oral health care, *JBR-BTR* 94 (5) (2011) 254–265.
- [2] J.B. Ludlow, L.E. Davies-Ludlow, S.L. Brooks, W.B. Howerton, Dosimetry of 3 CBCT devices for oral and maxillofacial radiology: CB Mercuray, NewTom 3 G and i-CAT, *Dentomaxillofac Radiol* 35 (4) (2006) 219–226.
- [3] J.B. Carter, J.D. Stone, R.S. Clark, J.E. Mercer, Applications of cone-beam computed tomography in oral and maxillofacial surgery: an overview of published indications and clinical usage in United States academic centers and oral and maxillofacial surgery practices, *J. Oral. Maxillofac Surg.* 74 (4) (2016) 668–679.
- [4] J.O. Agbaje, E.V. de Castele, A.S. Salem, D. Anumendem, I. Lambrichts, C. Politis, Tracking of the inferior alveolar nerve: its implication in surgical planning, *Clin. Oral. Investig.* 21 (7) (2017) 2213–2220.
- [5] R. Jacobs, M. Quiryren, M.M. Bornstein, Neurovascular disturbances after implant surgery, *Periodontol.* 66 (1) (2014) 188–202, 2000.
- [6] H. Ghaemina, G.J. Meijer, A. Soehardi, W.A. Borstlap, J. Mulder, O.J. Vlijmen, et al., The use of cone beam CT for the removal of wisdom teeth changes the surgical approach compared with panoramic radiography: a pilot study, *Int. J. Oral Maxillofac Surg.* 40 (8) (2011) 834–839.
- [7] B. Friedland, B. Donoff, T.B. Dodson, The use of 3-dimensional reconstructions to evaluate the anatomic relationship of the mandibular canal and impacted mandibular third molars, *J. Oral Maxillofac Surg.* 66 (8) (2008) 1678–1685.
- [8] Y.Y. Leung, L.K. Cheung, Risk factors of neurosensory deficits in lower third molar surgery: an literature review of prospective studies, *Int. J. Oral Maxillofac Surg.* 40 (1) (2011) 1–10.
- [9] M. Ueda, K. Nakamori, K. Shiratori, T. Igarashi, T. Sasaki, N. Anbo, et al., Clinical significance of computed tomographic assessment and anatomic features of the inferior alveolar canal as risk factors for injury of the inferior alveolar nerve at third molar surgery, *J. Oral Maxillofac Surg.* 70 (3) (2012) 514–520.
- [10] M.A. Pogrel, K.E. Goldman, Lingual flap retraction for third molar removal, *J. Oral Maxillofac Surg.* 62 (9) (2004) 1125–1130.
- [11] F. Van der Cruyssen, F. Peeters, T. Gill, A. De Laat, R. Jacobs, C. Politis, et al., Signs and symptoms, quality of life and psychosocial data in 1331 post-traumatic trigeminal neuropathy patients seen in two tertiary referral centres in two countries, *J. Oral Rehabil.* 47 (10) (2020) 1212–1221.
- [12] N.L. Gerlach, G.J. Meijer, T.J. Maal, J. Mulder, F.A. Rangel, W.A. Borstlap, et al., Reproducibility of 3 different tracing methods based on cone beam computed tomography in determining the anatomical position of the mandibular canal, *J. Oral Maxillofac Surg.* 68 (4) (2010) 811–817.
- [13] N.L. Gerlach, H. Ghaemina, E.M. Bronkhorst, S.J. Berge, G.J. Meijer, T.J. Maal, Accuracy of assessing the mandibular canal on cone-beam computed tomography: a validation study, *J. Oral Maxillofac. Surg.* 72 (4) (2014) 666–671.
- [14] R. Pauwels, R. Jacobs, S.R. Singer, M. Mupparapu, CBCT-based bone quality assessment: are Hounsfield units applicable? *Dentomaxillofac. Radiol.* 44 (1) (2015), 20140238.
- [15] O'Shea K., Nash R. An Introduction to Convolutional Neural Networks. Computing Research Repository, 2015.
- [16] A. Popovic, M. de la Fuente, M. Engelhardt, K. Radermacher, Statistical validation metric for accuracy assessment in medical image segmentation, *Int. J. Comput. Assist. Radiol. Surg.* 2 (3–4) (2007) 169–181.
- [17] O. Ronneberger, P. Fischer, Brox T. U-Net, Convolutional networks for biomedical image segmentation. Medical Image Computing and Computer-Assisted Intervention – MICCAI 2015, Lecture Notes in Computer Science, 2015, pp. 234–241.
- [18] K.D. Toennies, Segmentation and basic techniques. Guide to Medical Image Analysis - Methods and Algorithms, 1. 2 ed, Springer, London, 2017, pp. 208–247.
- [19] I. Balki, A. Amirabadi, J. Levman, A.L. Martel, Z. Emersic, B. Meden, et al., Sample-size determination methodologies for machine learning in medical imaging research: a systematic review, *Can. Assoc. Radiol. J.* 70 (4) (2019) 344–353.

- [20] J. Jaskari, J. Sahlsten, J. Jarnstedt, H. Mehtonen, K. Karhu, O. Sundqvist, et al., Deep learning method for mandibular canal segmentation in dental cone beam computed tomography volumes, *Sci. Rep.* 10 (1) (2020) 5842.
- [21] Y. Tsuji, T. Muto, J. Kawakami, S. Takeda, Computed tomographic analysis of the position and course of the mandibular canal: relevance to the sagittal split ramus osteotomy, *Int. J. Oral Maxillofac. Surg.* 34 (3) (2005) 243–246.
- [22] J. Larsen, L.K. Hansen, C. Svarer, M. Ohlsson, Design and regularization of neural networks: the optimal use of a validation set, in: *Proceedings of the 1996 IEEE Signal Processing Society Workshop*, IEEE, 1996.
- [23] 3D U-Net: learning dense volumetric segmentation from sparse annotation, in: Ö Çiçek, A Abdulkadir, S S Lienkamp, T Brox, O Ronneberger (Eds.), *Proceedings of the Medical Image Computing and Computer-Assisted Intervention*, Springer, 2016.
- [24] M.A. Rahman, Y. Wang, Optimizing intersection-over-union in deep neural networks for image segmentation. *advances in visual computing. Lecture Notes in Computer Science*, Springer, 2016, pp. 234–244.
- [25] D. Karimi, S.E. Salcudean, Reducing the Hausdorff distance in medical image segmentation with convolutional neural networks, *IEEE Trans. Med. Imaging* 39 (2) (2020) 499–513.
- [26] M. Beauchemin, K.P.B. Thomson, G. Edwards, On the Hausdorff distance used for the evaluation of segmentation results, *Canadian J. Remote Sens.* 24 (1) (1998) 3–8.
- [27] F.C. Monteiro, A.C. Campilho, A.C. Campilho, M. Kamel, Performance evaluation of image segmentation. *Image Analysis and Recognition. ICIAR 2006*, Springer, Portugal, 2006, pp. 248–259.
- [28] X. Zhang, X. Feng, P. Xiao, G. He, L. Zhu, Segmentation quality evaluation using region-based precision and recall measures for remote sensing images, *ISPRS J. Photogr. Remote Sens.* 102 (2015) 73–84.
- [29] D.M.W. Powers, Evaluation: from precision, recall and F-factor to ROC, informedness, markedness & correlation, *J. Machine Learn. Technol.* 2 (2011) 37–63.
- [30] G.H. Kwak, E.J. Kwak, J.M. Song, H.R. Park, Y.H. Jung, B.H. Cho, et al., Automatic mandibular canal detection using a deep convolutional neural network, *Sci. Rep.* 10 (1) (2020) 5711.
- [31] P. Lahoud, M. EzEldeen, T. Beznik, H. Willems, A. Leite, A. Van Gerven, et al., Artificial intelligence for fast and accurate 3D tooth segmentation on CBCT, *J. Endod.* (2021).
- [32] A.F. Leite, A.V. Gerven, H. Willems, T. Beznik, P. Lahoud, H. Gaeta-Araujo, et al., Artificial intelligence-driven novel tool for tooth detection and segmentation on panoramic radiographs, *Clin. Oral Investig.* (2020).
- [33] A.F. Leite, K.F. Vasconcelos, H. Willems, R. Jacobs, Radiomics and machine learning in oral healthcare, *Proteomics Clin. Appl.* 14 (3) (2020), e1900040.
- [34] R. Cop, *Automatic Teeth Thresholding in Cone Beam CT With Convolutional Neural Networks and Tooth Segmentation With the Watershed Transform*, University of Groningen, The Netherlands, 2018.
- [35] I.M. Zaki, W.M. Hamed, M.S. Ashmawy, Effect of CBCT dose reduction on the mandibular canal visibility: ex vivo comparative study, *Oral. Radiol.* 37 (2) (2021) 282–289.